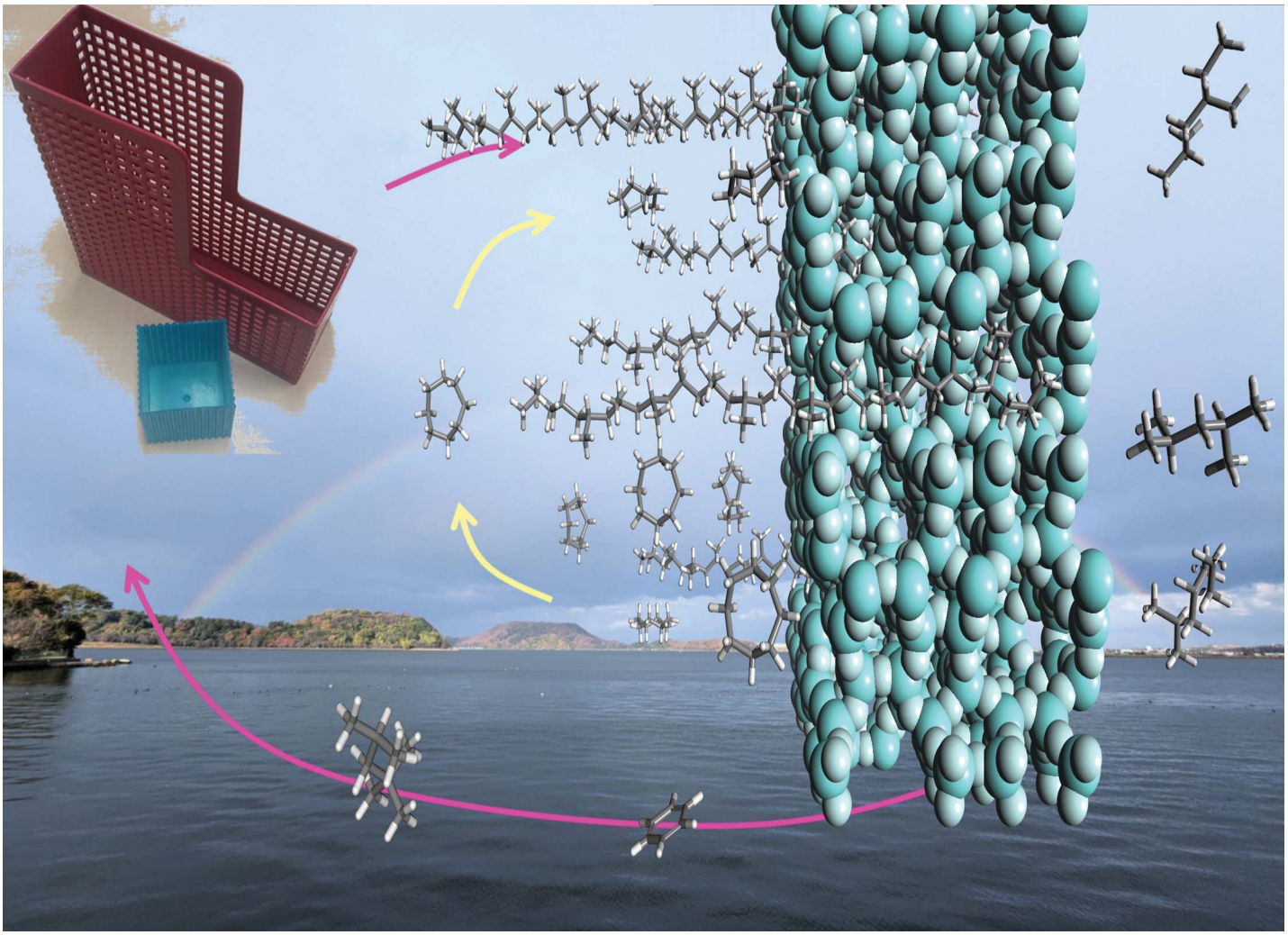

Showcasing research from Professor Katada's laboratory, Center for Research on Green Sustainable Chemistry, Tottori University, Japan.

Shape selective cracking of polypropylene on an H-MFI type zeolite catalyst with recovery of cyclooctane solvent

In the photo, you can see a rainbow over Koyama-ike lake near Tottori University. Tottori University has developed the first method to use shape selectivity to crack polymers while recovering the solvent. The polymers enter the micropores of zeolite and are cracked into naphtha, a raw material for plastics, which is then recycled. The solvent helps transport the polymer and heat, but the solvent with bulky molecular shape does not enter the micropores and is recovered, creating another cycle. This will be a rainbow bridge between waste and resources.

As featured in:

See Naonobu Katada *et al.*, *RSC. Sustainability.*, 2025, **3**, 890.

ROYAL SOCIETY OF CHEMISTRY

rsc.li/rscsus

Registered charity number: 207890

RSC Sustainability

ROYAL SOCIETY OF CHEMISTRY

PAPER

View Article Online
View Journal | View Issue

Cite this: *RSC Sustainability*, 2025, **3**, 890

Shape selective cracking of polypropylene on an H-MFI type zeolite catalyst with recovery of cyclooctane solvent†

Tomohiro Fukumasa,[a] Yuya Kawatani,[a] Hiroki Masuda,[a] Ikuto Nakashita,[a] Ryusei Hashiguchi,[a] Masanori Takemoto,[b] Satoshi Suganuma,[c] Etsushi Tsuji,[a] Toru Wakaihara[d] and Naonobu Katada*[a]

The use of hydrocarbon solvents for zeolite-catalyzed polyolefin cracking narrows the molecular weight distribution of the products, which enhances the efficiency of polyolefin chemical recycling to naphtha, a key precursor to polyolefins. However, solvent consumption remains a challenge. In this study, zeolite microporosity was used to achieve shape-selective polyolefin cracking while allowing solvent recovery. With an H-**MFI** type zeolite catalyst combined with cyclooctane as the solvent, polypropylene was selectively converted without cyclooctane reactivity. In a typical case, 84% of polypropylene was converted into C3-27 aliphatic and monocyclic aromatic compounds (equivalent to liquid petroleum gas, naphtha, kerosene, jet and diesel) with 79% selectivity, while 95% of cyclooctane was recovered. This study is the first to demonstrate solvent recyclability in polyolefin cracking on an acidic zeolite, contributing to the chemical recycling of polyolefin into its precursor, naphtha, with high selectivity facilitated by the presence of solvent but without solvent consumption.

Received 15th August 2024
Accepted 20th November 2024

DOI: 10.1039/d4su00484a

rsc.li/rscsus

Sustainability spotlight

Here we submit a paper "Shape Selective Cracking of Polypropylene on an H-**MFI** Type Zeolite Catalyst with Recovery of Cyclooctane Solvent", reporting a fact that polyolefin was selectively cracked into naphtha-related gaseous and liquid hydrocarbons over an **MFI**-zeolite catalyst with small micropores, while the solvent, cyclooctane, was mostly recovered. This will open a way for chemical recycling of polyolefins without consuming other materials contributing to sustainability in the plastic industry. The paper states that the reason for this phenomenon was the shape-selectivity due to the microporous structure. The contents are based on the sustainability concept and will gather interest of the readers of *RSC Sustainability*.

Introduction

Achieving a carbon-neutral society requires the exploration of alternatives to the two primary uses of petroleum: fuel and chemical resources. While petroleum-based fuels are being rapidly replaced by electricity, hydrogen, ammonia and synthetic fuels—often sourced from solar, wind or biophotosynthetic energy—the demand for petroleum-derived chemicals, especially plastics, remains high. In 2015, it was estimated that 300 million tons of plastic were discarded (landfilled or incinerated), of which approximately 100 million tons were recycled.[1] Expanding plastic recycling is critical for establishing a sustainable carbon cycle and protecting the marine environment.

Polyolefins (POs), such as polyethylene (PE) and polypropylene (PP), account for 60% of the plastics produced and consumed.[1] In actual waste, even after advanced sorting,[2] a variety of PO molecules with different chain lengths and microstructures remain. In the field of PO recycling, mechanical recycling is difficult because it involves separating the waste plastic and restoring the initial physicochemical properties of each polymer part. Therefore, chemical recycling is required to convert POs into hydrocarbons equivalent to their raw material, namely, naphtha.[3,4]

POs can undergo hydrogenolysis into small hydrocarbon molecules. For hydrogenolysis, noble metal catalysts, such as Ru[5] or Pt,[6] are required to upgrade POs into alkanes under

[a]*Center for Research on Green Sustainable Chemistry, Faculty of Engineering, Tottori University, 4-101 Koyama-cho Minami, Tottori 680-8552, Japan. E-mail: katada@tottori-u.ac.jp*

[b]*Department of Chemical System Engineering, School of Engineering, The University of Tokyo, 7-3-1 Hongo, Bunkyo-ku, Tokyo 113-8656, Japan*

[c]*Institute for Catalysis, Hokkaido University, Kita21, Nishi10, Kita-ku, Sapporo, Hokkaido, Japan*

[d]*Institute of Engineering Innovation, School of Engineering, The University of Tokyo. Department of Project, 2-11-16 Yayoi, Bunkyo-ku, Tokyo 113-8656, Japan*

† Electronic supplementary information (ESI) available: Compositions of solutions after PP cracking experiments, nitrogen adsorption isotherms, ^{29}Si NMR spectra and full width at half maximum of XRD. See DOI: https://doi.org/10.1039/d4su00484a

pressurized hydrogen. By contrast, POs are long-chain alkanes. The catalytic cracking of short-chain alkanes has been well studied and practiced since the early 20th century.[7–16] The most advanced catalysts for alkane cracking are acid-form (H-form) zeolites with framework types such as **FAU** and **MFI**.

Zeolites are a group of crystalline materials formed by a three-dimensional network of Si–O covalent bonds with micropores due to the framework topology. Some of the Si (oxidation number +4) in the framework is substituted by Al (+3), which generates a negative charge on the framework which can hold a cation. When the counter cation is H^+, the zeolite is called H-, proton-, acidic- or acid-form zeolite, and the proton plays the role of Brønsted acid. The number of Brønsted acid sites on the H-form zeolite is principally equal to the number of Al atoms.[17–19] This enables the adjustment of the concentration of Brønsted acid sites and the distance between two Brønsted acid sites, which strongly influences the catalytic selectivity and life.[20] The acid strength (the ability to stabilize the counter cation[21]) is dependent on the framework topology.[19,22] Some specific framework topologies, *e.g.*, **MFI**, show strong Brønsted acidity owing to the structural feature generating strong compression from both ends of the Si–OH–Al group.[21–23]

H-form zeolites have been used in various chemical reactions, including conversion of artificial[24–37] and bio-derived[20,38] polymers. H-form zeolites have high potential for recycling and extended catalyst life, reducing the costs of catalysts because the framework components are only Si, O and Al. These components form strong covalent bonds and exhibit durability against high temperatures, humidity, and reduction/oxidation conditions. Even on zeolites, the Al–O–Si–O–Al bond induces dealumination and structural distortion.[18,39,40] However, the Al–O–Si–O–Al bond is not formed with <*ca.* 1 mol kg^{-1} of Al in the **MFI** framework.[41] Therefore, an **MFI** type zeolite with <*ca.* 1 mol kg^{-1} of Al (called high silica ZSM-5 zeolite, corresponding to >16 of the Si/Al molar ratio) does not lose crystallinity at temperatures less than approximately 1273 K,[42] suggesting structural stability at such a reaction temperature of 673 K and durability against calcination typically at 873 K for regeneration of the active sites. Previous studies have found that this type of zeolite exhibits recyclability as a catalyst for the degradation of polymers such as sucrose and cellulose.[20] Zeolites are microporous, which limits the diffusion rates of reactants; however, even with this drawback, the strong Brønsted acidity of these zeolites allows the catalytic cracking of alkanes at *ca.* 773 K, where product selectivity can be controlled.[43] The catalytic cracking of POs has already been attempted.[24,26–37,44–52] The mechanism of acid catalysis for PO cracking has been elucidated using metal chloride catalysts,[53] which are not practical owing to the difficulty in separating the catalyst from the product. A narrow molecular weight distribution was observed on an **MFI** type zeolite catalyst.[25] Based on the reaction conditions and nature of the catalyst, two types of reactions are possible: (1) combined pyrolysis (non-catalytic thermal decomposition) and catalytic cracking of the pyrolysis product,[54,55] and (2) direct cracking of POs over a solid catalyst.[56,57]

Previous reports have indicated that the use of solvents provides advantages in the catalytic cracking of polymers.[54,58–61] In the reaction field, a pure PO forms a highly viscous liquid, causing problems such as local overheating of the reactor wall and overdecomposition into carbonaceous materials. Solvents (or simply co-existing liquids) suppress the viscosity of the reactants and promote thermal and material diffusion.[58,60] Because the reaction temperature can be easily controlled in the presence of solvent, the product is expected to have a narrow molecular weight distribution. The use of solvents is also advantageous for the separation and transportation of practical waste prior to the reaction.[62]

However, methods using solvents for PO cracking have a fatal drawback. The solvent (any organic compound) reacts and is consumed in the same manner as the polymer as long as it is in contact with the active sites, making it impossible to recycle the carbon. In limited cases, attempts have been made to recover the solvent. To recycle carbon fibers from carbon fibre-reinforced polymer (CFRP) composites, the resin matrix was decomposed by cleaving the ester bonds under mild conditions (433 K), and the relatively stable monoethanolamine solvent was recovered.[63] Decomposition of polyethylene terephthalate (PET) was achieved under mild conditions (<403 K) while suppressing the decomposition of the imidazole solvent.[64] The chemical stability of ionic liquids has been applied for the recovery of solvents during polymer decomposition.[65] All of these known techniques combine reaction conditions suitable for the decomposition of the target polymer with a solvent that is stable under those conditions. However, the decomposition of POs (long-chain alkanes), which are chemically inert, requires extreme reaction conditions, such as a high temperature of 673 K.

In this study, we aimed to develop a method based on the shape selectivity owing to the microporosity of zeolites. Because it has been reported that PO cracking proceeds within micropores,[37] a combination of a zeolite with small micropores and a solvent with a bulky molecular shape was used to ensure shape selectivity of the reactants for the selective cracking of POs and selective recovery of the solvent (Scheme 1). For the first time, we combined an **MFI** type zeolite with small micropores (diameter *ca.* 0.55 nm)[66] as a catalyst and cyclooctane with a bulky molecular shape (*ca.* 0.8 nm)[67] as a solvent, which will be the first step in developing a method for the chemical recycling of POs without consuming other materials.

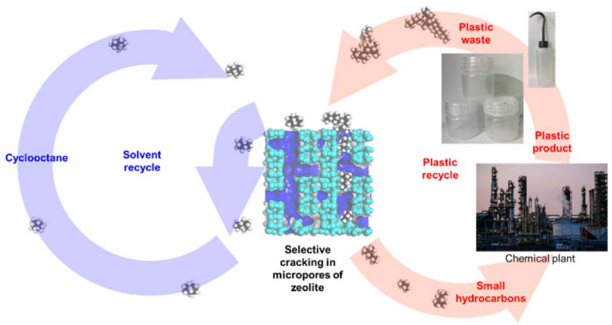

Scheme 1 Assumed material flow during shape selective cracking in micropores of zeolite.

To the best of our knowledge, the effect of micropore characteristics on the polymer cracking activity and product distribution has been reported;[56,68–73] however, the selective conversion of polymers and solvent recovery based on the shape selectivity of the reactants have not been reported. Additionally, we tested a series of zeolites treated with a base (alkali) in the presence of amorphous silica for PO cracking. In addition to changes in the external surface area by the base treatment,[74] we expected the modification of the local structure, such as recrystallization,[75] by the presence of amorphous silica. Based on the change in PO cracking activity caused by the silica alkali treatment, the location of PO cracking and the origin of selectivity were discussed.

Results and discussion

Quality of the parent MFI sample

X-ray diffraction (XRD) showed that the parent sample (denoted as "0" in Fig. 1) had a strong-intensity diffraction pattern attributed to the **MFI** crystal structure. Nitrogen adsorption at 77 K of the parent sample (denoted as "0" in Fig. S1†) showed a type I isotherm[76] and high micropore volume (0.13 $cm^3\ g^{-1}$), as shown in Table 1. These indicate that the parent sample had a highly crystalline **MFI** framework topology.

The ^{27}Al nuclear magnetic resonance (NMR) spectrum of the parent sample (denoted as "0" in Fig. 2) showed a major resonance at 57 ppm (four-coordinated Al) with a small proportion at 4 ppm (six-coordinated Al). Moreover, the framework Al content (▼ at 0 mol $kg_{zeolite}^{-1}$ of NaOH in Fig. 3, indicating the sample before the alkali treatment) was similar to the total Al content (△ at 0 mol $kg_{zeolite}^{-1}$ of NaOH in Fig. 3) as estimated from ^{29}Si NMR (Fig. S2†). These observations indicate that most of the Al was incorporated into the framework of the parent **MFI** sample. Table 1 shows that the amount of Brønsted acid sites (0.72 mol kg^{-1}) was close to the amount of Al (0.9 mol kg^{-1}), and the amount of Lewis acid was negligible, which confirms that most of the Al atoms were incorporated into the framework and served as Brønsted acid sites.

In conclusion, the parent sample was highly crystalline **MFI** zeolite, which had a high proportion of framework Al atoms that served as Brønsted acid sites.

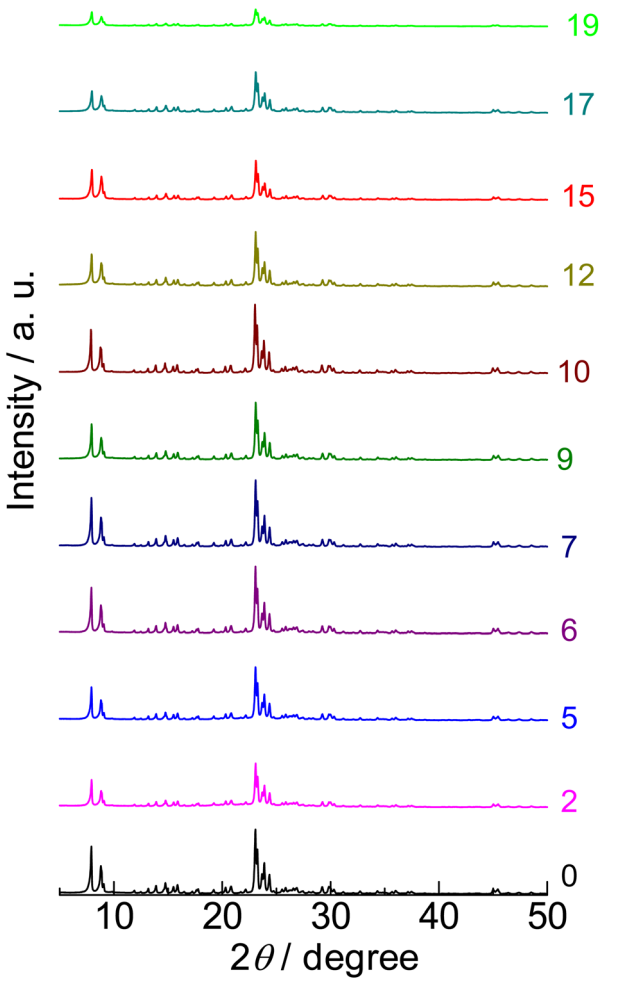

Fig. 1 X-ray diffraction patterns of (0) parent MFI and (2)–(19) silica-alkali-treated MFI under Cu Kα X-ray irradiation (0.154 nm). The digits indicate the amount of NaOH used for the silica-alkali treatment in units of mol $kg_{zeolite}^{-1}$.

Change in textural properties by silica-alkali treatment

The alkali (base) treatment of zeolite partially dissolves the zeolite and forms wormhole-like mesopores, resulting in an increase in the external surface area (total area of meso- and macropore walls).[74] Wakihara *et al.* found that recrystallization proceeded in the region close to the external surface of zeolite in a basic solution containing a silica source.[75] We used this silica-alkali treatment method to maintain high crystallinity in the region near the external surface. This gradually changed the properties of the external surface as follows.

Fig. 3 (○) shows that the solid recovery after the alkali treatment at 453 K decreased when the amount of base (NaOH) increased, indicating that a part of the parent solid (amorphous silica + parent **MFI** zeolite) was dissolved in the base. The Al content (△) gradually increased with increasing NaOH, suggesting that the dissolution of the SiO_2 component in the base occurred prior to the dissolution of the Al-containing part. The dissolution of amorphous silica, which had only a pure component, is speculated to occur in the low NaOH concentration region. Meanwhile, the framework Al content (▼) was almost constant in the region of 0–10 mol $kg_{zeolite}^{-1}$ of NaOH but increased in higher NaOH amount regions (12 mol $kg_{zeolite}^{-1}$), suggesting the dissolution of zeolite (aluminosilicate) framework in >12 mol $kg_{zeolite}^{-1}$ of NaOH. In very high alkali concentration regions (>15 mol $kg_{zeolite}^{-1}$ of NaOH), the difference between the total and framework Al contents became significantly large, and ^{27}Al NMR (Fig. 2) showed a relatively large proportion of the six-coordinated Al, indicating that some of the Al dislodged from the framework remained in the solid as extra-framework Al species.

XRD (Fig. 1) confirmed that only the **MFI** crystalline phase was observed throughout the silica-alkali treatments with different NaOH amounts. However, the XRD intensity was suppressed to *ca.* 68% by the silica-alkali treatment with 2 mol

Table 1 Employed catalysts and precursors

Sample name	Description	Si/Al molar ratio	[Al]/mol kg^{-1}	Origin	Micropore volume[a]/$cm^3\ g^{-1}$	External surface area[b] (area of meso- and macropore wall)/$m^2\ g^{-1}$	Brønsted acid amount/mol kg^{-1}	Lewis acid amount/mol kg^{-1}
Parent **MFI**	ZSM-5 zeolite with **MFI** framework topology	15	0.9	EX-122 from Mizusawa Industrial Chemicals, Ltd., ion exchanged into NH_4-form	0.13	9	0.72	0.00
Silica-alkali-treated **MFI**	Modified ZSM-5 zeolite with **MFI** framework topology	15[c]	0.9[c]	Parent **MFI** was treated with NaOH solution in the co-presence of amorphous silica, ion exchanged into NH_4-form	0.12[c]	39[c]	0.89[c]	0.00[c]
Amorphous silica	Used for silica-alkali treatment	∞	0	Reolosil from Tokuyama Corp.	0.013	434	0.00	0.00
Beta	Zeolite β with **Beta** framework topology	14	1.1	930NHA from Tosoh Corp.	0.22	33	0.83	0.04
ASA	Amorphous silica-alumina	5.7	2.6	N631-L from JGC Catalysts and Chemicals Ltd	0	483	0.17	0.09

[a] Determined from N_2 capillary condensation capacity at $p/p_0 = 0.005$ and 77 K.[96,97] [b] For zeolites, the external surface area is determined by the *t*-plot method,[95] while for amorphous silica and silica-alumina, the total surface area is determined by the BET method.[99] [c] Values of silica-alkali-treated **MFI** prepared with 12 mol $kg_{zeolite}^{-1}$ of NaOH as a representative sample.

$kg_{zeolite}^{-1}$ of NaOH, then gradually recovered up to *ca.* 100% in the region of 7–10 mol $kg_{zeolite}^{-1}$ of NaOH and finally decreased again with a further increase in the amount of NaOH, as shown in Fig. 4 (●). The crystallite size was estimated from the width of diffraction (Fig. S3†) using the Scherrer equation,[77] as shown in Fig. 4 (△). It was maintained in the region of 0–12 mol $kg_{zeolite}^{-1}$ of NaOH, and further increase in the NaOH amount reduced the crystallite size. The reduction of crystallite size may affect the decrease in XRD intensity in the same region (>12 mol $kg_{zeolite}^{-1}$ of NaOH); however, the weak intensity of XRD peaks in the low NaOH amount region (2–5 mol $kg_{zeolite}^{-1}$) was presumably due to low crystallinity.

Scanning electron microscopy (SEM) analysis (Fig. 5) showed large crystals of parent **MFI** (0) and small particles around the **MFI** crystallites treated with 2–5 mol $kg_{zeolite}^{-1}$ of NaOH. It is presumed that the particles were remaining amorphous silica which was added for the silica-alkali treatment. At 9 mol $kg_{zeolite}^{-1}$, the small particles (amorphous silica) diminished, and the morphology of the solid was similar to that of the parent **MFI**. At >12 mol $kg_{zeolite}^{-1}$, holes (mesopores) with a diameter <10 nm were observed.

As shown in Table 1, the micropore volume of parent **MFI** was high (0.130 $cm^3\ g^{-1}$) as stated in the previous subsection, while that of amorphous silica was low (0.013 $cm^3\ g^{-1}$). In contrast, the external surface area of parent **MFI** was low (9 $m^2\ g^{-1}$), whereas that of amorphous silica was high (434 $m^2\ g^{-1}$). As shown in Fig. 6, the pore diameter of amorphous silica was distributed in the 10–200 nm region; some of them should be ascribed to the slits among the particles.

By the alkali treatment with 2–5 mol $kg_{zeolite}^{-1}$ of NaOH, the micropore volume was decreased, as shown in Fig. 7 (●), whereas the micropore volume was recovered at >6 mol $kg_{zeolite}^{-1}$ of NaOH up to the level equivalent to the parent **MFI**. At 2–5 mol $kg_{zeolite}^{-1}$ of NaOH, meso- and macropores with diameters of 10–200 nm were observed (Fig. 6), resulting in a high volume of mesopores with diameters >9 nm (Fig. 7, ▽). At 6–9 mol $kg_{zeolite}^{-1}$ of NaOH, the meso-/macropore volume was low. Fig. 6 shows that, at >10 mol $kg_{zeolite}^{-1}$ of NaOH, new mesopores with diameters <5 nm, were generated. The distribution peak of pore diameter around 4 nm calculated from the desorption branch is ascribable to the cavitation of nitrogen filling the pore entrances,[78] and therefore, the actual diameters on these samples are estimated to be less than the values where the peaks were observed, that is, less than several nanometers. Consequently, the volume of mesopores with diameters <9 nm (Fig. 7, ▲) increased in the region of 10–15 mol $kg_{zeolite}^{-1}$ of NaOH, with a maximum at 15 mol $kg_{zeolite}^{-1}$, and decreased with further increases in NaOH.

These observations clarify the changes in the chemical composition and textural properties due to the silica-alkali treatments with different NaOH amounts.

(1) The added amorphous silica was gradually dissolved by the alkali treatment, but at 2–5 mol $kg_{zeolite}^{-1}$ of NaOH, the amorphous silica remained. The obtained solid was a mixture of amorphous silica and zeolite, as shown by the SEM results and the low crystallinity observed in the XRD; hence its micropore volume was lower than that of the parent **MFI**. Meso-/

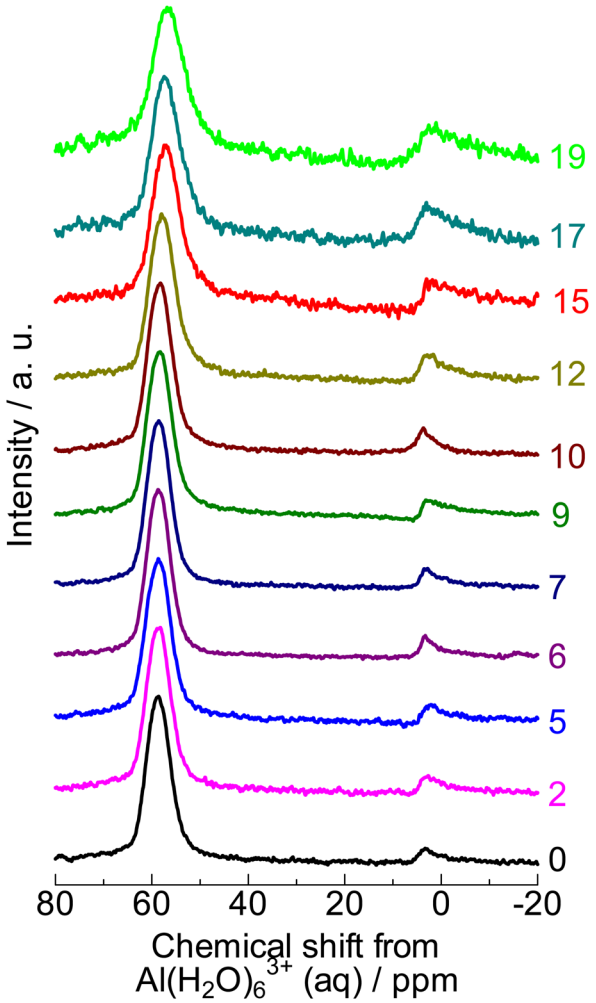

Fig. 2 ^{27}Al NMR spectra of (0) parent **MFI** and (2)–(19) silica-alkali-treated **MFI**. The digits indicate the amount of NaOH used for the silica-alkali treatment in units of mol $kg_{zeolite}^{-1}$.

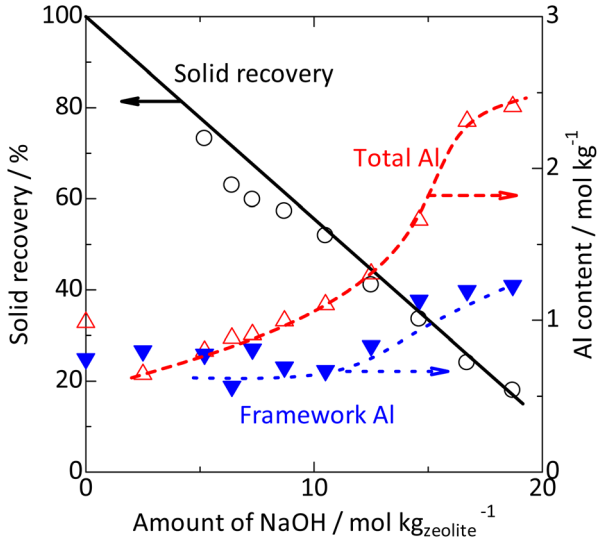

Fig. 3 Solid recovery (○), and changes in total (△, from ICP) and framework [▼, from ^{29}Si NMR (Fig. S2†)] Al contents by silica-alkali treatment of **MFI** zeolite. *: Recovery = Weight ratio of (recovered solid)/(used zeolite + silica).

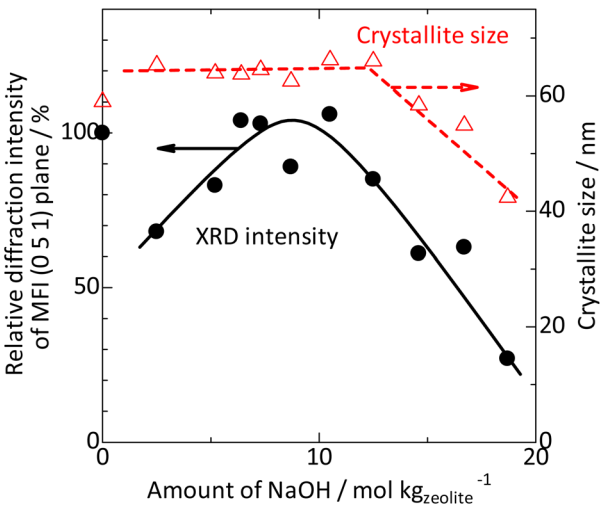

Fig. 4 Intensity (●) and crystallite size (△) estimated using the Scherrer equation[63] from the full width at half maximum (Fig. S3†) of the diffraction peak ascribed to the **MFI** (0 5 1) plane (2θ = 23.1°) observed by X-ray diffraction (Fig. 1). Intensity is normalized by the value on parent **MFI** (EX-122).

macropores with diameters >9 nm, ascribed to the amorphous silica, were observed, whereas mesopores with diameters <9 nm were hardly observed.

(2) At 6–9 mol $kg_{zeolite}^{-1}$ of NaOH, most of the added amorphous silica was dissolved by alkali treatment, with the resultant solid showing high crystallinity, high micropore volume, and low mesopore volume. This agrees with the fact that the solid mainly consisted of highly crystalline **MFI** zeolite.

(3) At 10–15 mol $kg_{zeolite}^{-1}$ of NaOH, wormhole-like mesopores in nanometric dimensions were generated by the alkali treatment of the **MFI** zeolite in the presence of silicate species dissolved in the solvent.

(4) At >11 mol $kg_{zeolite}^{-1}$ of NaOH, desilication of the **MFI** zeolite proceeded to increase the framework Al content. The crystal size was reduced, as shown by XRD.

(5) In the extremely high alkali concentration region (>15 mol $kg_{zeolite}^{-1}$ of NaOH), destruction of the **MFI** structure proceeded owing to significant desilication, resulting in the low crystallinity shown by XRD and a large proportion of extra-framework Al species shown by ^{27}Al NMR.

The catalytic activity for 1,3,5-triisopropylbenzene cracking was negligible on the parent zeolite and amorphous silica. It was increased by the silica-alkali treatment in the range of 6–10 mol $kg_{zeolite}^{-1}$ of NaOH, and high conversion was maintained with further increases in NaOH, as shown in Fig. 8 (▲). These results suggest that the number of the Brønsted acid sites on the external surface was mainly increased by the treatments with 6–10 mol $kg_{zeolite}^{-1}$ of NaOH. Notably, as explained previously, the silica-alkali-treated **MFI** with 6–9 mol $kg_{zeolite}^{-1}$ of NaOH mainly consisted of highly crystalline **MFI** zeolite. However, the activity of Brønsted acid sites on the external

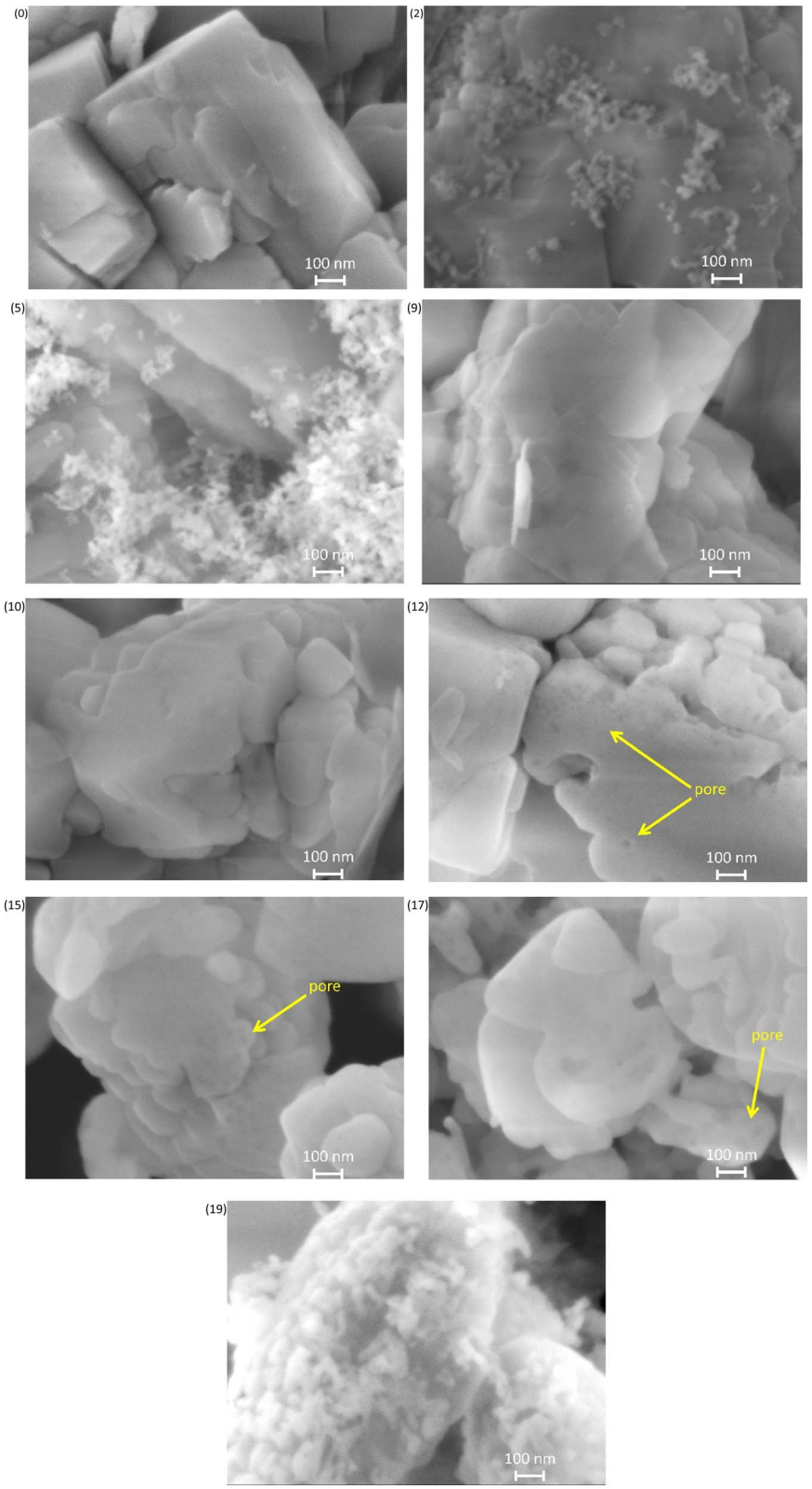

Fig. 5 Field emission scanning electron microscope (FE-SEM) images of (0) parent **MFI** and (2)–(19) silica-alkali-treated **MFI**. The digit in parentheses indicates the amount of NaOH used for the silica-alkali treatment in units of mol $kg_{zeolite}^{-1}$.

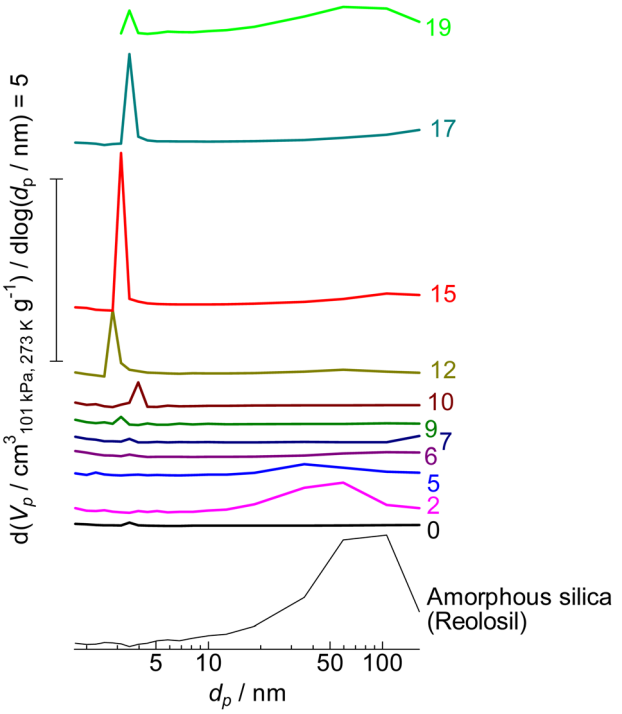

Fig. 6 Mesopore diameter distribution of (0) parent **MFI** and (2)–(19) silica-alkali-treated **MFI** and amorphous silica (Reolosil) estimated by the BJH method.[75] The digits indicate the amount of NaOH used for the silica-alkali treatment in units of mol $kg_{zeolite}^{-1}$. V_p and d_p represent the pore volume and diameter, respectively.

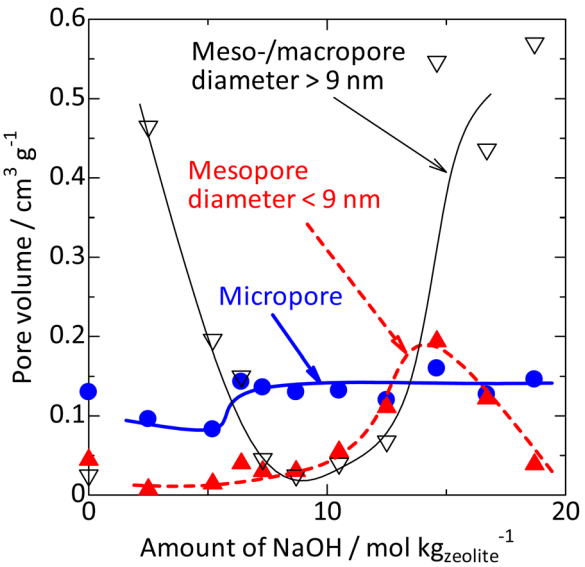

Fig. 7 Changes in volumes of micropores (●), mesopores with diameter <9 nm (▲) and meso-/macropores >9 nm (▽) by silica-alkali treatment of **MFI** zeolite. The micropore volume was calculated from the amount of nitrogen filling the micropores[73,74] from the adsorption branch, while the mesopore volume was estimated using the BJH method[75] from the desorption branch (mesopore diameter distribution is shown in Fig. 6), based on the nitrogen adsorption/desorption isotherm at 77 K (Fig. S1†).

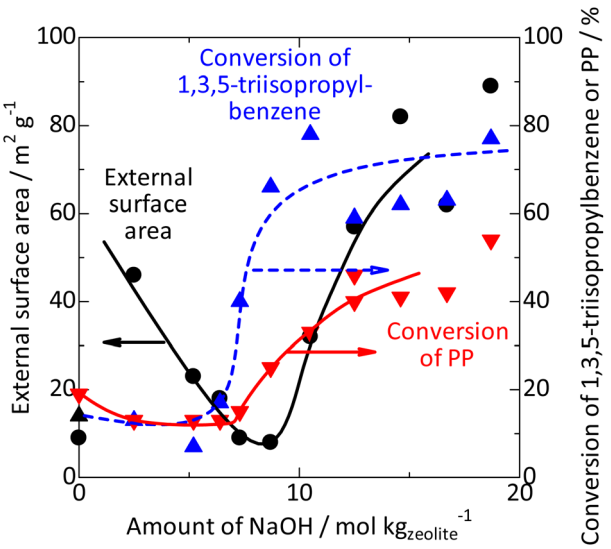

Fig. 8 Change in the external surface area (●) and catalytic activities for 1,3,5-triisopropylbenzene cracking (▲) and PP cracking (conversion at 663 K, ▼) by silica-alkali treatment of **MFI** zeolite.

surface was much higher than that of the parent **MFI**. It is likely that the external surface of the parent **MFI** was covered by an inert layer, which was highly siliceous and/or amorphous and dissolved in the low alkali concentration region, similar to the amorphous silica.

Consequently, we obtained a series of **MFI** samples whose chemical and external surface properties were modified. As shown in Fig. 8, the activity of Brønsted acid sites on the external surface (▲) was generated at 6–10 mol $kg_{zeolite}^{-1}$ of NaOH, whereas the external surface area (●) was significantly increased in a slightly larger NaOH amount region, 9–15 mol $kg_{zeolite}^{-1}$. The framework Al content (Fig. 3, ▼) increased in a higher NaOH amount region, >11 mol $kg_{zeolite}^{-1}$.

Location of PP cracking

It is known that polyolefins, such as PP, are cracked on acidic zeolites. In this study, we attempted to clarify the location of this reaction. We tested the following four hypotheses.

(1) In the initial stage of the reaction, the PP molecules are bulky and large; therefore, thermal pyrolysis proceeds in solution without a catalyst, producing polymer fragments.

(2) The PP cracking is first catalysed by the Brønsted acid sites on the external surface of zeolite, and the acid sites within the micropores mainly contribute to the subsequent cracking of the formed medium-length alkanes.

(3) The molecular chains of PP penetrate the micropores of the zeolite, and cracking occurs within the pores. Micropores restrict the diffusion of long molecules; however, when only the end of the molecule is inserted into the pore, diffusion is sufficiently fast because of the short length of the alkyl moiety within the pore. Therefore, the reaction mainly proceeds in micropores close to the pore mouths.

(4) The diffusion of PP is sufficiently faster than the reaction, and the reaction proceeds throughout the micropores.

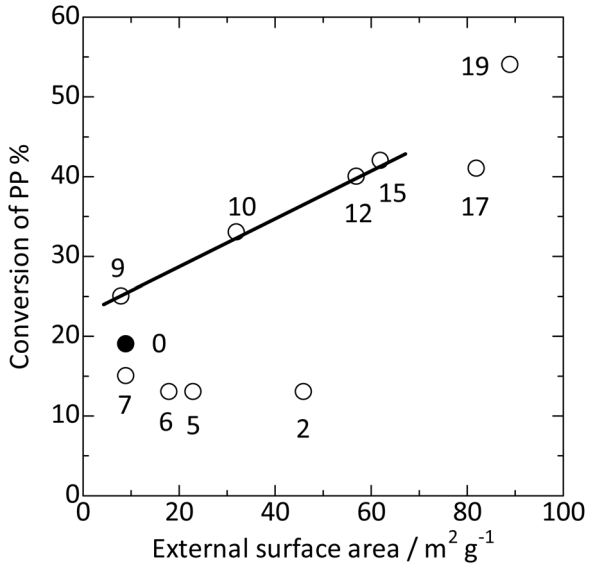

Fig. 9 Plots of PP conversion at 663 K against external surface area. The conversion on parent MFI is shown using ●, whereas those on the silica-alkali-treated MFI samples are shown using ○. The digits indicate the amount of NaOH used for the silica-alkali treatment in units of mol $kg_{zeolite}^{-1}$.

As shown in the previous subsection, a series of samples with different chemical and external surface properties were obtained, allowing experiments to test the above hypotheses.

At 663 K, cracking of PP (0.25 g) was tested in cyclooctane (1 g) without a catalyst, and negligible reactivity (conversion <1%) was observed. Thus, Hypothesis (1) was rejected. Fig. 8 (▼) shows the change in catalytic activity for PP cracking with respect to the NaOH amount employed for the alkali treatment. Considerable activity was observed on the unmodified **MFI**. In the region of <9 mol $kg_{zeolite}^{-1}$ of NaOH, the activity did not increase significantly. In this region, the activity of Brønsted acid sites on the external surface was increased by the silica-alkali treatment, as shown in Fig. 8 (▲). Thus, the PP cracking activity is not related to the activity of Brønsted acid sites on the external surface. This suggests that the contribution of the acid sites on the external surface to PP cracking was not dominant, which refutes Hypothesis (2). The low activity of the acid sites on the external surface of the **MFI** type zeolite for the polymer pyrolysis and related reactions has been reported.[79] As shown in Fig. 8 (▼), silica-alkali treatment in the >9 mol $kg_{zeolite}^{-1}$ region significantly enhanced the PP cracking activity. In this region, the external surface area increased, as shown in Fig. 8 (●). Fig. 9 shows a good relationship between the PP cracking activity and the external surface area; simultaneously, its vertical intercept was not zero. These observations suggested that PP cracking predominantly occurred in the micropores of the **MFI** type zeolite. However, PP cracking activity was not correlated with the framework Al content (increased at >11 mol $kg_{zeolite}^{-1}$ of NaOH, as shown in Fig. 3 ▼), demonstrating that the activity was not dependent on the total Brønsted acidity. This is consistent with the fact that PP cracking occurs in a limited portion of the zeolite. Because a high external surface area enhanced the activity, Hypothesis (3) was supported, and Hypothesis (4) was rejected. It is likely that PP cracking occurred mainly in the micropores, and the region near the pore mouth was mainly responsible for the reaction.

Tsubota *et al.* also reported the dependency of low-density polyethylene (LDPE) cracking activity on the physicochemical properties of **MFI** type zeolite to indicate that at least a part of LDPE cracking proceeded in the micropores.[37]

The kinetic diameter of monomethyl-branched alkane is regarded to be 0.50 nm,[80] smaller than the diameter of micropores of **MFI** type zeolite (10-ring, *ca.* 0.55 nm).[67] Thus, it is reasonable that a part of the PP molecule penetrates the micropores of **MFI** type zeolite. PP forms a three-dimensional network with entanglements and cross-links consisting of multiple chains, even at a high temperature of 673 K. It is speculated that the head of the molecule penetrated the micropores, and the reaction proceeded in the region close to the pore entrance.

Catalytic activities for cracking of cyclohexane and polypropylene

Hereafter, the effects of the reactant polymer, solvent, catalyst, and reaction temperature will be shown through experiments

Table 2 Reaction conditions in Entries 1–13

Entry	Polymer (0.25 g)	Solvent (1 g)	Catalyst (0.05 g)	Reaction temperature/K[a]
1	No	Cyclooctane	No	673
2	PP	Cyclooctane	No	673
3	No	Cyclooctane	Parent **MFI** zeolite	673
4	PP	No	Parent **MFI** zeolite	673
5	PP	Cyclooctane	Parent **MFI** zeolite	673
6	PP	Hexadecane	Parent **MFI** zeolite	673
7	PP	Cyclooctane	**Beta** zeolite	673
8	PP	Cyclooctane	ASA[b]	673
9	PP	Cyclooctane	Silica-alkali-treated **MFI** zeolite[c]	673
10	PP	Cyclooctane	Silica-alkali-treated **MFI** zeolite[c]	693
11	LLDPE	Cyclooctane	Silica-alkali-treated **MFI** zeolite[c]	673
12	GPPS	Cyclooctane	Silica-alkali-treated **MFI** zeolite[c]	673
13	PP	No	Silica-alkali-treated **MFI** zeolite[c]	673

[a] Reaction time was 1 h in all entries. [b] Amorphous silica-alumina N631-L. [c] **MFI** zeolite treated with silica and alkali (12 mol_{NaOH} $kg_{zeolite}^{-1}$).

Table 3 Conversion of reactants observed in reaction tests at 673 K for 1 h

Entry	Reactant	Catalyst	Cyclooctane conversion/%	PP conversion/%
1	Cyclooctane 1.0 g	No	2.3	—
2	Cyclooctane 1.0 g + PP 0.25 g	No	1.8	4.3
3	Cyclooctane 1.0 g	Parent **MFI** 0.05 g	24	—
4	PP 0.25 g	Parent **MFI** 0.05 g	—	57.3

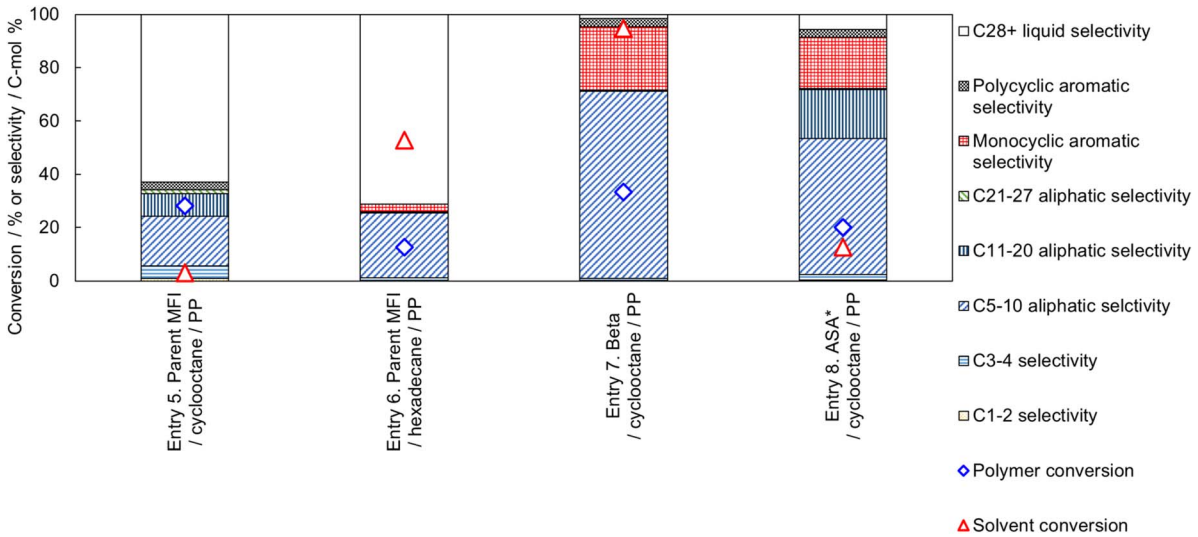

Fig. 10 Effect of catalyst and solvent combination on the cracking performance (PP and solvent conversion, and selectivity) of PP (0.25 g) with solvent (1 g) and catalyst (0.05 g) at 673 K for 1 h, where ASA* denotes amorphous silica alumina N631-L.

involving the variation of these variables, as in Entries 1–13 in Table 2.

As shown in Table 3, heating of pure cyclooctane (Entry 1) and a mixture of cyclooctane and PP (Entry 2) without a catalyst at 673 K for 1 h resulted in negligible conversion of cyclooctane and PP. These indicate that the non-catalytic reaction of alkanes under the experimental conditions has a negligible influence on the discussion below, and the reactions observed below were mainly the catalytic cracking of alkanes and not pyrolysis (non-catalytic thermal decomposition).

Entry 3 in Table 3 shows that the cyclooctane conversion in the presence of parent **MFI** zeolite as a catalyst was also negligible. It is presumed that because of its bulky molecular shape, cyclooctane did not enter the micropores of the **MFI** type zeolite. The kinetic diameter of cyclooctane is 0.80 nm,[66] larger than the micropore diameter of the **MFI** type zeolite (*ca.* 0.55 nm),[67] and is in agreement with the inactivity of cyclooctane on the **MFI** type zeolite. In contrast, heating of pure PP with the parent **MFI** at 673 K for 1 h (Entry 4) resulted in a high conversion of PP. This agrees with the previous subsection, where the conversion of PP was observed at a slightly lower temperature of 663 K. Thus, pure cyclooctane was not converted, while pure PP was converted using the **MFI** type zeolite catalyst.

Next, we investigated the reaction of a mixture of PP and cyclooctane on the parent **MFI** zeolite, as shown in Fig. 10 (Entry 5). The conversion of cyclooctane was very low (3%), and most of the cyclooctane was recovered, while the PP conversion was 28%. Most of the products were liquid (C5-40) hydrocarbons.

In Entry 6, a linear alkane (hexadecane) was used as the solvent for PP cracking on the parent **MFI** zeolite catalyst. The conversion of hexadecane was high (53%), while the PP conversion was suppressed (13%) compared to that in cyclooctane (Entry 5, 28%). The high reactivity of hexadecane on the **MFI** zeolite suggests that hexadecane penetrates the micropore of **MFI** and occupies the cavities to suppress the diffusion and conversion of PP molecules. In Entries 7 and 8, catalysts with larger pore sizes (**Beta** type zeolite and amorphous silica-alumina) showed higher conversions of cyclooctane.

Thus, a high PP conversion and low solvent conversion were observed only when cyclooctane and **MFI** type zeolite were used as the solvent and catalyst, respectively. The cyclooctane molecule (kinetic diameter 0.80 nm)[66] is larger than the micropore of **MFI** (10-ring, *ca.* 0.55 nm).[67] The use of narrow solvent molecule (hexadecane, whose kinetic diameter should be equivalent to other linear alkanes, 0.43 nm)[80] or the use of catalysts with larger pore sizes (**Beta**: 12-ring, 0.74 × 0.64 nm[81] or amorphous silica-alumina N631-L: averagely 4 nm[82]) showed no selectivity. As explained in the previous subsection, PP cracking proceeds mainly in the micropores, even in the **MFI** type zeolite, which has the smallest pore size among the presently used catalysts. These facts clearly indicate that the selective reaction of PP in the PP-cyclooctane mixture is caused by reactant shape

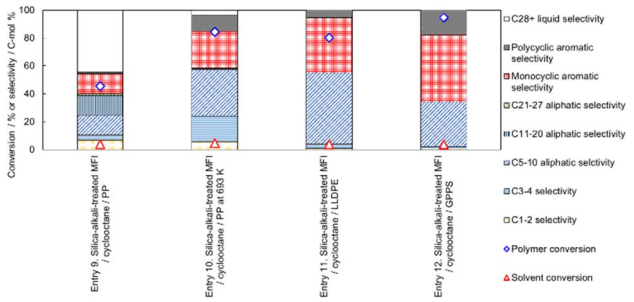

Fig. 11 Influence of reaction temperature (Entries 9 and 10, PP cracking at 673 and 693 K, respectively) and influence of reactant polymers (Entries 9, 11 and 12, PP, LLDPE and GPPS cracking, respectively, at 673 K) on polymer cracking performance catalyzed by silica-alkali-treated **MFI** for 1 h with polymer (0.25 g), cyclooctane as the solvent (1 g) and silica-alkali-treated **MFI** (prepared with 12 mol_{NaOH} $kg_{zeolite}^{-1}$) as the catalyst (0.05 g).

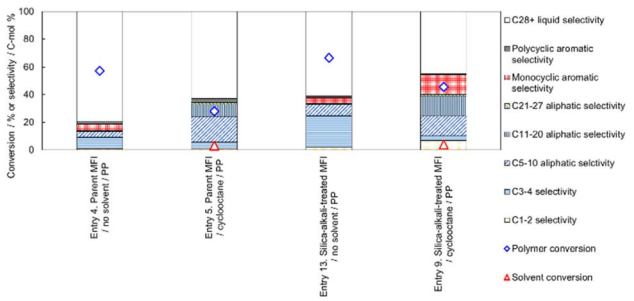

Fig. 12 Comparison of PP cracking performances in the absence (Entries 4 and 13) and presence (Entries 5 and 9) of cyclooctane solvent catalyzed by parent **MFI** (Entries 4 and 5) and silica-alkali-treated **MFI** (Entries 13 and 9, prepared with 12 mol_{NaOH} $kg_{zeolite}^{-1}$) at 673 K for 1 h with PP as the polymer (0.25 g), cyclooctane as the solvent (1 g) and a catalyst (0.05 g).

selectivity. Only molecules smaller than the catalyst pores reacted selectively, while molecules bulkier than the pores were recovered without any reaction.

In the field of polymer cracking, shape selectivity (transition state shape selectivity or product shape selectivity in terms of the reaction mechanism), in which the product distribution is influenced by the porous structure, has been known.[70,83] However, to the best of our knowledge, the contribution of reactant shape selectivity to the selective recovery of the solvent has not been reported. Herein, we report the first example of reactant shape selectivity with a microporous catalyst applicable to the chemical recycling of POs without consuming other materials (solvents), as shown in Scheme 1.

Entry 9 in Fig. 11 shows the catalytic performance of silica-alkali-treated **MFI** (12 mol_{NaOH} $kg_{zeolite}^{-1}$) for PP cracking in cyclooctane. Compared to Entry 5 in Fig. 10 (parent **MFI**), the PP conversion on the silica-alkali-treated **MFI** was higher, in agreement with the previous subsection, where the enhancement of activity for PP cracking by the increase in the external surface area was demonstrated. The silica-alkali-treated **MFI** zeolite was then tested at a slightly higher temperature (693 K) for PP cracking (Entry 10). The PP conversion reached 84%, and the sum of C3-27 aliphatic and monocyclic hydrocarbons selectivities was 79%, meaning that most of the PP was converted into valuable hydrocarbons (LPG, naphtha, kerosene, jet, and diesel), while the cyclooctane conversion was 5% (95% of cyclooctane was recovered). Entry 11 indicates that the selective cracking can be applied to linear low-density polyethylene (LLDPE). On the silica-alkali-treated **MFI**, 80% of PE (here LLDPE) was converted into mainly C5-10 aliphatic and monocyclic aromatic hydrocarbons, while only 4% of cyclooctane was consumed. Entry 12 shows 95% of PS (here general purpose polystyrene, GPPS) was converted. In this case, it was speculated that the high reactivity of alkylaromatic hydrocarbons resulted in the non-catalytic cracking of PS, and the intermediates reacted on the zeolite. It was confirmed that the cyclooctane conversion was low (4%) in this case also and that selective cracking was applicable to PO and PS. Throughout Entries 9–12, the conversion of cyclooctane was $\leq$5%, presumably because the micropore of the silica-alkali-treated **MFI** was also small owing to the **MFI** framework topology.

Fig. 12 shows the effect of the presence of cyclooctane on the selectivity of **MFI** type zeolite-catalysed PP cracking. Comparison of Entries 4 (without solvent) and 5 (with cyclooctane solvent) shows that, over the parent **MFI** zeolite catalyst, the use of the solvent significantly increased the C5-20 aliphatic selectivity, whereas C3-4 and C28+ selectivities were suppressed. The decrease in the amount of small (C3-4) hydrocarbons in the presence of cyclooctane is ascribable to the lower reaction progress shown by the lower PP conversion in Entry 5, whereas the decrease in C28+ liquid selectivity reveals that the chain length distribution of products was narrowed by adding cyclooctane. In addition, also on the silica-alkali-treated **MFI** catalyst, the formation of C3-4 and C28+ hydrocarbons observed without the catalyst (Entry 13) was significantly suppressed in the presence of cyclooctane (Entry 9). The use of solvents for PO cracking contributes to high mass and heat transfer and a homogeneous temperature distribution.[54] In the presence of cyclooctane, these effects probably result in a narrow product distribution. A narrow product distribution is necessary to produce a specific region of a hydrocarbon mixture, such as naphtha. Fig. 12 shows the advantage of selectivity achieved by the addition of solvent.

Notably, high selectivity for valuable hydrocarbon compounds was achieved by the reaction in cyclooctane, although cyclooctane itself was not present in the micropores where PO cracking occurred. As mentioned above, the primary role of the solvent in PO cracking is probably to improve thermal and mass transportation. The high selectivity observed in the presence of the solvent outside the reaction field (micropore) indicates that the solvent influenced heat and mass transportation but did not directly influence the chemistry of the active site or the reaction mechanism.

For the short chain alkane (C3-8) cracking, the active site has been clarified to be a strong Brønsted acid site based on the relationship between activity and acidic properties[15,43,84–87] and dependence of activation enthalpy on ammonia desorption enthalpy.[43,88–91] Since strong Brønsted acidity is required to

initiate the reaction, nonclassical carbonium ion formation is considered the initial step in the reaction. C–C bond cleavage of the carbonium ion leads to the formation of a carbenium ion and a short alkane pair, as in reaction (1).[92] The former is further decomposed into a shorter carbenium ion and alkene pair, as in reaction (2).[12,93] In reaction (2), tertiary carbenium ions are preferred over secondary and primary carbenium ions; thus, alkanes longer than C3 are preferentially formed, unlike non-catalytic radical reactions where all C–C bonds have similar probabilities for cleavage, resulting in the considerable formation of C1-2 fragments.

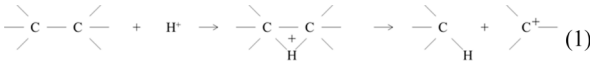
(1)

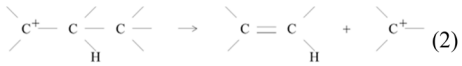
(2)

As PO is an alkane, PO cracking catalysed by acidic zeolite, as shown in the present study, is believed to have the same reaction mechanism. The low selectivity of C1-2 products observed in the reactions catalyzed by the acidic zeolite is consistent with the mechanism. The low activity of ASA (amorphous silica-alumina) with lower Brønsted acid strength[23,82] is also in agreement with the speculated mechanism.

In contrast, the PO polymer forms a three-dimensional network. As stated in the previous subsection, it is speculated that the head of a molecule penetrates the micropores to contact the Brønsted acid sites on the pore walls.

This work shows the possibility of a new sustainable method for polymer recycling that does not consume solvents and has high selectivity for the polymer precursor owing to the presence of the solvent. In the small-scale experiments, almost complete recovery of the solvent (>95%) was achieved; however, in a real process the efficiency of several steps, such as separation of the catalyst from the hydrocarbon mixture, separation of the solvent from the product, and purification of the solvent for repeated use, is an issue. Therefore, a life cycle assessment (LCA) of the new process based on a comprehensive evaluation of these efficiencies is necessary in the next research stage.

In addition, we have not yet tested the repeated use of the catalyst; therefore we have no experimental evidence about the life, degradation and recyclability of the catalyst because the recycling test requires complex experimental procedures for the complete collection of the solid catalyst after the reaction in a small reaction tube and separation of the zeolite from the remaining solid polymer in the present reaction system. Therefore, information on the recyclability of the catalyst, energy and resource consumption, and economic efficiency has not been obtained. Here we can discuss only the general trend of the catalytic life of **MFI** type zeolites, which typically exhibit low solubility in organic media, high stability at temperatures such as 1373 K[42] in the low Al concentration region (<*ca.* 1 mol kg^{-1}). Therefore, it is reasonable to expect that the **MFI** type zeolite is durable under the reaction conditions (673 K) and the calcination conditions required for the regeneration of active sites (typically 873 K). In addition, compared to other zeolites, **MFI** type zeolites are known to have a distinct long life for reactions such as the transalkylation[91] and cracking[94] of hydrocarbons. It is therefore expected that the **MFI** type zeolites can be repeatedly used for polymer cracking. It is predicted that contaminants in practical waste such as alkaline salts and nitrogen-containing organic compounds with basicity could neutralise the Brønsted acid sites to lose the catalytic activity, and therefore a more important research subject is the applicability and recyclability for the cracking of practical waste POs containing these contaminants. Here we showed only fundamental findings, and the evaluation of the recyclability of the catalyst should be the subject of the next study.

Experimental

Catalyst preparation

NH_4-ZSM-5 zeolite (aluminosilicate with an **MFI** framework topology, Si/Al molar ratio of 15, EX-122 from Mizusawa Industrial Chemicals, Ltd) was used as the parent **MFI** sample. Table 1 lists its important physicochemical properties. Amorphous silica (Reolosil from Tokuyama Corp.) was used as a feedstock, and its properties are also shown in Table 1.

For the silica-alkali treatment, the parent **MFI** (6 g) was added to a mixture of amorphous silica (4 g), NaOH (FUJIFILM Wako Pure Chemical Corp), and 60 cm^3 of ion-exchanged water, stirred in an autoclave at 453 K for 2 h, washed and filtered. The obtained Na-form of zeolite (3.5 g) was twice ion-exchanged with an aqueous solution (300 cm^3) of NH_4NO_3 (24 g) at 338 K for 4 h.

In addition, zeolite β (aluminosilicate with a **Beta** framework topology, hereafter **Beta**) and amorphous silica-alumina (hereafter ASA) were employed as catalysts (shown in Table 1).

The NH_4-form zeolites were calcined at 813 K for 4 h in air, and the obtained H-form zeolites were used for the PO cracking reaction.

Structure and texture analysis. XRD analysis was performed using a Rigaku Ultima IV diffractometer with a Cu Kα X-ray source operated at a voltage of 40 kV and a current of 40 mA. The crystallite size was estimated using the Scherrer equation[77] from the full width at half maximum of the diffraction peak ascribed to the **MFI** (0 5 1) plane ($2\theta = 23.1°$) in the XRD. The surfaces and morphologies of the samples were observed using a field-emission scanning electron microscope (FE-SEM, JSM-IT800, JEOL) with an accelerating voltage of 5 kV.

Nitrogen adsorption/desorption isotherms were measured at 77 K using Microtrac-BEL BELSorp-max or BELSorp-mini equipment after evacuation at 573 K for 1 h. The micropore volume was calculated by the *t*-plot method,[95] and the value was confirmed to be similar to the volume of liquid nitrogen showing capillary condensation[96,97] at $p/p_0 = 0.01$ and $T = 77$ K, where p, p_0 and T are the pressure of nitrogen, vapor pressure of nitrogen, and temperature, respectively. Here, the volume of pores with diameters 2–50 nm is termed the mesopore volume and was calculated by the Barrett–Joyner–Halenda (BJH) method.[98] The external surface area, that is, the area of mesopore and macropore walls in this study, was calculated by the *t*-plot method.[95]

Solid-state magic angle spinning nuclear magnetic resonance (MAS NMR) spectra were recorded using a JNM-ECZ 400 instrument (JEOL). The ^{29}Si dipolar decoupling (DD) MAS NMR spectra were measured at 79.42 MHz with a $\pi/2$ pulse length of 3.3 μs, a relaxation delay of 30 s, and a spinning frequency of 10 kHz. The ^{27}Al MAS NMR spectra were measured at 104.17 MHz with a $\pi/2$ pulse length of 2.97 μs, a relaxation delay of 5.0 s, and a spinning frequency of 14 kHz.

Catalytic cracking of PO

Cyclooctane and hexadecane, purchased from FUJIFILM Wako Pure Chemical Corp., were used as solvents. PP (Mw: weight average molecular weight = 370 000 and Mn: number average molecular weight = 32 000), LLDPE (Mw = 110 000 and Mn = 39 000), and GPPS (Mw = 240 000 and Mn = 15 000) were supplied by Japan Petroleum and Carbon Neutral Fuels Energy Center. The molecular weight distributions were analyzed using gel permeation chromatography as detailed in Fig. S4.† The polymer (0.25 g) and catalyst (0.05 g) were placed in a solvent (1 g) in a stainless-steel tube (i.d. 10 mm, volume 3.6 cm^3), and the gas phase was purged with N_2. It was sealed, and heated using an electric furnace while maintaining the temperature of the thermocouple attached to the stainless-steel tube at 663–693 K for 1 h. After cooling, the stainless-steel tube was connected to a gas syringe, and the volume of the formed gas was measured at atmospheric pressure and room temperature. The gaseous products were analyzed by gas chromatograph with a flame ionization detector (FID-GC). The solid and liquid were then separated, and the liquid was analyzed by an internal standard method using a two-dimensional FID-GC. The solid was washed with pentane, dried, and weighed.

Conclusions

Alkali (NaOH) treatment of the **MFI** type zeolite in the presence of amorphous silica suggests that PP cracking mainly proceeded in the region near the entrances of the micropores. As previously reported for other hydrocarbon solvents, the use of cyclooctane as a solvent provided a narrow molecular weight distribution of the products in the PP cracking on the **MFI** catalyst. The combination of the cyclooctane solvent and **MFI** catalyst resulted in the selective cracking of PP, while most of the cyclooctane was recovered. Using a linear alkane (hexadecane) as the solvent or a catalyst with large pores (**Beta** type zeolite or amorphous silica-alumina) resulted in high conversion of both solvent and PP. These observations indicate that selective PP cracking is based on the shape selectivity caused by the 10-ring micropores of **MFI** and the bulky molecular shape of cyclooctane. The products were valuable hydrocarbons. For example, the reaction of PP (0.25 g) with cyclooctane (0.1 g) on silica-alkali-treated **MFI** (0.05 g) at 693 K for 1 h converted 84% of PP into C3-27 aliphatic and monocyclic aromatic compounds (equivalent to LPG, naphtha, kerosene, jet, and diesel) with 79% selectivity, while 95% of cyclooctane was recovered. The newly discovered shape-selective cracking of PO with solvent recovery will contribute to a sustainable process for the chemical recycling of PO into its precursor, naphtha, with high selectivity facilitated by the presence of solvent without consuming the solvent.

Data availability

The data supporting this article have been included as part of the ESI.†

Author contributions

Tomohiro Fukumasa: data curation, investigation, methodology, visualization, writing – original draft, Yuya Kawatani: data curation, investigation, methodology, visualization, writing – original draft, Hiroki Masuda: data curation, investigation, methodology, visualization, Ikuto Nakashita: data curation, investigation, Ryusei Hashiguchi: data curation, investigation, Masanori Takemoto: investigation, methodology, visualization, Satoshi Suganuma: methodology, validation, writing – review & editing, Etsushi Tsuji: methodology, validation, writing – review & editing, Toru Wakaihara: conceptualization, funding acquisition, methodology, project administration, writing – review & editing, and Naonobu Katada: conceptualization, data curation, formal analysis, funding acquisition, methodology, project administration, validation, visualization, writing – original draft, writing – review & editing.

Conflicts of interest

There are no conflicts to declare.

References

1 R. Geyer, J. R. Jambeck and K. L. Law, *Sci. Adv.*, 2017, **3**, e1700782.
2 R. Noll, in *Laser-Induced Breakdown Spectroscopy: Fundamentals and Applications*, ed. R. Noll, Springer Berlin Heidelberg, Berlin, Heidelberg, 2012, pp. 275–386, DOI: 10.1007/978-3-642-20668-9_14.
3 C. G. Schirmeister and R. Mulhaupt, *Macromol. Rapid Commun.*, 2022, **43**, 2022247.
4 I. Vollmer, M. J. F. Jenks, M. C. P. Roelands, R. J. White, T. Harmelen, P. Wild, G. P. Laan, F. Meirer, J. T. F. Keurentjes and B. M. Weckhuysen, *Angew. Chem., Int. Ed.*, 2020, **59**, 15402–15423.
5 Y. Nakaji, M. Tamura, S. Miyaoka, S. Kumagai, M. Tanji, Y. Nakagawa, T. Yoshioka and K. Tomishige, *Appl. Catal., B*, 2021, **285**, 119805.
6 P. Zhao, W. Guo, Z. Gui, J. Jiang, Z. Zhu, J.-J. Li, L. Zhao, J. Zhou and Z. Xi, *ACS Sustain. Chem. Eng.*, 2024, **12**, 5738–5752.
7 P. B. Venuto and R. T. Habib, *Catal. Rev.:Sci. Eng.*, 1978, **18**, 1.
8 A. Corma, J. B. Monton and A. V. Orchilles, *Appl. Catal.*, 1985, **16**, 59–74.
9 H. G. Karge, V. Mavrodinova, Z. K. Zheng and H. K. Beyer, *Appl. Catal.*, 1991, **75**, 343–358.

10 A. R. Songip, T. Masuda, H. Kuwahara and K. Hashimoto, *Energy Fuels*, 1994, **8**, 136–140.
11 V. B. Kazansky, M. V. Frash and R. A. vanSanten, *Appl. Catal., A*, 1996, **146**, 225–247.
12 S. M. Babitz, M. A. Kuehne, H. H. Kung and J. T. Miller, *Ind. Eng. Chem. Res.*, 1997, **36**, 3027–3031.
13 S. Kotrel, M. P. Rosynek and J. H. Lunsford, *J. Phys. Chem. B*, 1999, **103**, 818–824.
14 P. Borges, R. R. Pinto, M. A. N. D. A. Lemos, F. Lemos, J. C. Vedrine, E. G. Derouane and F. R. Ribeiro, *J. Mol. Catal. A: Chem.*, 2005, **229**, 127–135.
15 N. Katada, S. Nakata, S. Kato, K. Kanehashi, K. Saito and M. Niwa, *J. Mol. Catal. A: Chem.*, 2005, **236**, 239–245.
16 F. Lonyi, A. Kovacs and J. Valyon, *J. Phys. Chem. B*, 2006, **110**, 1711–1721.
17 N. Katada, H. Igi, J. H. Kim and M. Niwa, *J. Phys. Chem. B*, 1997, **101**, 5969–5977.
18 N. Katada, Y. Kageyama and M. Niwa, *J. Phys. Chem. B*, 2000, **104**, 7561–7564.
19 M. Niwa, N. Katada and K. Okumura, in *Characterization and Design of Zeolite Catalysts*, Springer, Heidelberg, 2010, pp. 9–27.
20 H. Li, S. Yang, A. Riisager, A. Pandey, R. S. Sangwan, S. Saravanamurugan and R. Luque, *Green Chem.*, 2016, **18**, 5701–5735.
21 N. Katada, *Mol. Catal.*, 2018, **458**, 116–126.
22 N. Katada, K. Suzuki, T. Noda, G. Sastre and M. Niwa, *J. Phys. Chem. C*, 2009, **113**, 19208–19217.
23 N. Katada, K. Yamamoto, M. Fukui, K. Asanuma, S. Inagaki, K. Nakajima, S. Suganuma, E. Tsuji, A. Palcic, V. Valtchev, P. S. Petkov, K. Simeonova, G. N. Vayssilov and Y. Kubota, *Microporous Mesoporous Mater.*, 2022, **330**, 111592.
24 R. C. Mordi, J. Dwyer and R. Fields, *Polym. Degrad. Stab.*, 1994, **46**, 57–62.
25 J. Aguado, J. L. Sotelo, D. P. Serrano, J. A. Calles and J. M. Escola, *Energy Fuels*, 1997, **11**, 1225–1231.
26 S. C. Cardona and A. Corma, *Appl. Catal., B*, 2000, **25**, 151–162.
27 E. Y. Hwang, J. R. Kim, J. K. Choi, H. C. Woo and D. W. Park, *J. Anal. Appl. Pyrolysis*, 2002, **62**, 351–364.
28 J. R. Kim, Y. A. Kim, J. H. Yoon, D. W. Park and H. C. Woo, *Polym. Degrad. Stab.*, 2002, **75**, 287–294.
29 A. Marcilla, A. Gómez, J. A. Reyes-Labarta, A. Giner and F. Hernández, *J. Anal. Appl. Pyrolysis*, 2003, **68–69**, 467–480.
30 Q. Zhou, L. Zheng, Y. Z. Wang, G. M. Zhao and B. Wang, *Polym. Degrad. Stab.*, 2004, **84**, 493–497.
31 A. Durmus, S. N. Koç, G. S. Pozan and A. Kasgöz, *Appl. Catal., B*, 2005, **61**, 316–322.
32 K. Pyra, K. A. Tarach and K. Gora-Marek, *Appl. Catal., B*, 2021, **297**, 120408.
33 A. Santoso, A. Sholikhah, S. Sumari, M. R. Asrori, A. R. Wijaya, R. Retnosari and I. B. Rachman, *J. Renewable Mater.*, 2022, **10**, 2781–2789.
34 J. Mensah, P. H. Yan, A. Rawal, A. F. Lee, K. Wilson, N. Robinson, M. L. Johns, E. Kennedy and M. Stockenhuber, *ChemCatChem*, 2024, **16**, e202300884.
35 S. D. Xu, J. H. Tang and L. Fu, *Langmuir*, 2024, **40**, 3984–4000.
36 N. H. Nazarloo, O. Zabihi, K. Shirvanimoghaddam, M. Ahmadi and M. Naebe, *ChemCatChem*, 2024, **16**, e202300909.
37 S. Tsubota, S. Kokuryo, K. Tamura, K. Miyake, Y. Uchida, A. Mizusawa, T. Kubo and N. Nishiyama, *Catal. Sci. Technol.*, 2024, **14**, 1369–1374.
38 Z. Yu, H. Wu, Y. Li, Y. Xu, H. Li and S. Yang, *Ind. Eng. Chem. Res.*, 2020, **59**, 16970–16986.
39 N. Katada, T. Kanai and M. Niwa, *Microporous Mesoporous Mater.*, 2004, **75**, 61–67.
40 N. Katada, T. Takeguchi, T. Suzuki, T. Fukushima, K. Inagaki, S. Tokunaga, H. Shimada, K. Sato, Y. Oumi, T. Sano, K. Segawa, K. Nakai, H. Shoji, P. Wu, T. Tatsumi, T. Komatsu, T. Masuda, K. Domen, E. Yoda, J. N. Kondo, T. Okuhara, Y. Kageyama, M. Niwa, M. Ogura, M. Matsukata, E. Kikuchi, N. Okazaki, M. Takahashi, A. Tada, S. Tawada, Y. Kubota, Y. Sugi, Y. Higashio, M. Kamada, Y. Kioka, K. Yamamoto, T. Shouji, Y. Arima, Y. Okamoto and H. Matsumoto, *Appl. Catal., A*, 2005, **283**, 63–74.
41 D. Barthomeuf, *J. Phys. Chem.*, 1993, **97**, 10092–10096.
42 S. P. Zhdanov, N. N. Feoktistova, N. I. Kozlova and I. G. Polyakova, *Bull. Acad. Sci. USSR, Div. Chem. Sci.*, 1985, **34**, 2463–2466.
43 N. Katada, S. Sota, N. Morishita, K. Okumura and M. Niwa, *Catal. Sci. Technol.*, 2015, **5**, 1864–1869.
44 A. Marcilla, J. C. García-Quesada, S. Sánchez and R. Ruiz Femenia, *J. Anal. Appl. Pyrolysis*, 2005, **74**, 387–392.
45 D. Fraczak, *Przem. Chem.*, 2018, **97**, 299–304.
46 I. Muhammad and G. Manos, *ACS Sustain. Chem. Eng.*, 2022, **10**, 15824–15837.
47 S. B. Zhang, M. Li, Z. Y. Zuo and Z. Q. Niu, *Green Chem.*, 2023, **25**, 6949–6970.
48 R. Tiwari, N. Azad, D. Dutta, B. R. Yadav and S. Kumar, *Sci. Total Environ.*, 2023, **881**, 163433.
49 Y. W. Yang, R. M. Pan and S. A. Yong, *Fuel*, 2024, **361**, 130734.
50 Q. Xu, J. H. Zhu, B. C. Wu, G. Z. Jin, Y. P. Liu, A. H. Huang, C. Y. Tian and Y. T. Luo, *J. Energy Inst.*, 2024, **113**, 101556.
51 L. An, Z. L. Kou, R. J. Li and Z. Zhao, *Catalysts*, 2024, **14**, 212.
52 K. d. J. Mesquita, J. C. Pinto and H. P. Pacheco, *Macromol. React. Eng.*, 2024, **18**, 2300061.
53 W. Zhang, H. Yao, R. Khare, P. R. Zhang, B. D. Yang, W. D. Hu, D. Ray, J. Z. Hu, D. M. Camaioni, H. M. Wang, S. Kim, M. S. Lee, M. L. Sarazen, J. G. Chen and J. A. Lercher, *Angew. Chem., Int. Ed.*, 2024, **63**, e202319580.
54 J. M. Arandes, J. Erena, M. J. Azkoiti, D. Lopez-Valerio and J. Bilbao, *Fuel Process. Technol.*, 2004, **85**, 125–140.
55 Y. Peng, X. Wang, L. Fan, Q. Zhang, X. Cui, X. Tian, Q. Wu, K. Cobb, R. Ruan, H. Tu, J. Yang and Y. Wang, *J. Cleaner Prod.*, 2023, **418**, 138039.
56 J. Wang, J. C. Jiang, Y. J. Sun, Z. P. Zhong, X. B. Wang, H. H. Xia, G. H. Liu, S. S. Pang, K. Wang, M. Li, J. M. Xu, R. Ruan and A. J. Ragauskas, *Energy Convers. Manage.*, 2019, **200**, 112088.

57 A. C. Jerdy, L. Trevisi, M. Monwar, M. A. González-Borja, R. Abbott, L. Lobban and S. Crossley, *Appl. Catal., B*, 2023, **337**, 122986.
58 S. Wu, K. Xu, L. Jiang and L. Wang, *AASRI Procedia*, 2014, **7**, 3–7.
59 S. H. Ng, *Energy Fuels*, 1995, **9**, 216–224.
60 J. Aguado, D. P. Serrano, G. Vicente and N. Sanchez, *J. Polym. Environ.*, 2006, **14**, 375–384.
61 D. J. Machhi, B. Modhera and P. A. Parikh, *J. Mater. Cycles Waste Manage.*, 2023, **25**, 3005–3020.
62 Y. B. Zhao, X. D. Lv and H. G. Ni, *Chemosphere*, 2018, **209**, 707–720.
63 Q. Zhao, L. An, C. Li, L. Zhang, J. Jiang and Y. Li, *Compos. Sci. Technol.*, 2022, **224**, 109461.
64 T. Thiounn and R. C. Smith, *J. Polym. Sci.*, 2020, **58**, 1347–1364.
65 T. Christoff-Tempesta and T. H. Epps, *ACS Macro Lett.*, 2023, **12**, 1058–1070.
66 L. M. Chua, I. Hitchcock, R. S. Fletcher, E. M. Holt, J. Lowe and S. P. Rigby, *J. Catal.*, 2012, **286**, 260–265.
67 R. Le Van Mao, S. T. Le, D. Ohayon, F. Caillibot, L. Gelebart and G. Denes, *Zeolites*, 1997, **19**, 270–278.
68 O. Akin, R. J. Varghese, A. Eschenbacher, J. Oenema, M. S. Abbas-Abadi, G. D. Stefanidis and K. M. Van Geem, *J. Anal. Appl. Pyrolysis*, 2023, **172**, 106036.
69 H. Shafaghat, S. Gulshan, A. C. Johansson, P. Evangelopoulos and W. H. Yang, *Appl. Surf. Sci.*, 2022, **605**, 154734.
70 M. M. Hasan, N. Batalha, G. Fraga, M. H. M. Ahmed, L. Pinard, M. Konarova, S. Pratt and B. Laycock, *Sustainable Energy Fuels*, 2022, **6**, 1587–1602.
71 A. Farooq, S. Valizadeh, G. H. Rhee, J. Lee, J. Jae, S. C. Jung, W. H. Chen and Y. K. Park, *Energy Convers. Manage.*, 2022, **261**, 115652.
72 Y. M. Kim, J. Jeong, S. Ryu, H. W. Lee, J. S. Jung, M. Z. Siddiqui, S. C. Jung, J. K. Jeon, J. Jae and Y. K. Park, *Energy Convers. Manage.*, 2019, **195**, 727–737.
73 Y. K. Park, M. Z. Siddiqui, Y. Kang, A. Watanabe, H. W. Lee, S. J. Jeong, S. Kim and Y. M. Kim, *Catalysts*, 2018, **8**, 656.
74 M. Ogura, S. Y. Shinomiya, J. Tateno, Y. Nara, M. Nomura, E. Kikuchi and M. Matsukata, *Appl. Catal., A*, 2001, **219**, 33–43.
75 T. Wakihara, A. Ihara, S. Inagaki, J. Tatami, K. Sato, K. Komeya, T. Meguro, Y. Kubota and A. Nakahira, *Cryst. Growth Des.*, 2011, **11**, 5153–5158.
76 K. S. W. Sing, *Pure Appl. Chem.*, 1985, **57**, 603–619.
77 A. L. Patterson, *Phys. Rev.*, 1939, **56**, 978–982.
78 C. J. Rasmussen, A. Vishnyakov, M. Thommes, B. M. Smarsly, F. Kleitz and A. V. Neimark, *Langmuir*, 2010, **26**, 10147–10157.
79 C. Hu, H. Zhang, S. Wu and R. Xiao, *Energy Convers. Manage.*, 2020, **210**, 112678.
80 H. H. Funke, A. M. Argo, J. L. Falconer and R. D. Noble, *Ind. Eng. Chem. Res.*, 1997, **36**, 137–143.
81 T. O. Bok, E. P. Andriako, E. E. Knyazeva and I. I. Ivanova, *RSC Adv.*, 2020, **10**, 38505–38514.
82 N. Katada, Y. Kawaguchi, K. Takeda, T. Matsuoka, N. Uozumi, K. Kanai, S. Fujiwara, K. Kinugasa, K. Nakamura, S. Suganuma and M. Nanjo, *Appl. Catal., A*, 2017, **530**, 93–101.
83 J. Gancedo, H. Q. Li, J. S. Walz, L. Faba, S. Ordóñez and G. W. Huber, *Appl. Catal., A*, 2024, **669**, 119484.
84 N. Katada, Y. Kageyama, K. Takahara, T. Kanai, H. A. Begum and M. Niwa, *J. Mol. Catal. A: Chem.*, 2004, **211**, 119–130.
85 J. S. Jung, T. J. Kim and G. Seo, *Korean J. Chem. Eng.*, 2004, **21**, 777–781.
86 T. Noda, K. Suzuki, N. Katada and M. Niwa, *J. Catal.*, 2008, **259**, 203–210.
87 K. Okumura, T. Tomiyama, N. Morishita, T. Sanada, K. Kamiguchi, N. Katada and M. Niwa, *Appl. Catal., A*, 2011, **405**, 8–17.
88 J. Y. Shen and A. Auroux, in *Fluid Catalytic Cracking Vi: Preparation and Characterization of Catalysts*, ed. M. Occelli, 2004, vol. 149, pp. 35–70.
89 N. Katada, K. Suzuki, T. Noda, W. Miyatani, F. Taniguchi and M. Niwa, *Appl. Catal., A*, 2010, **373**, 208–213.
90 M. Niwa, K. Suzuki, N. Morishita, G. Sastre, K. Okumura and N. Katada, *Catal. Sci. Technol.*, 2013, **3**, 1919–1927.
91 K. Nakamura, R. Mizuta, S. Suganuma, E. Tsuji and N. Katada, *Catal. Commun.*, 2017, **102**, 103–107.
92 S. Kotrel, H. Knözinger and B. C. Gates, *Microporous Mesoporous Mater.*, 2000, **35–36**, 11–20.
93 W. M. Zhang and P. G. Smirniotis, *J. Catal.*, 1999, **182**, 400–416.
94 B. Bensafi, N. Chouat and F. Djafri, *Coord. Chem. Rev.*, 2023, **496**, 215397.
95 A. Galarneau, F. Villemot, J. Rodriguez, F. Fajula and B. Coasne, *Langmuir*, 2014, **30**, 13266–13274.
96 D. Mitsuyoshi, K. Kuroiwa, Y. Kataoka, T. Nakagawa, M. Kosaka, K. Nakamura, S. Suganuma, Y. Araki and N. Katada, *Microporous Mesoporous Mater.*, 2017, **242**, 118–126.
97 K. Nakajima, S. Suganuma, E. Tsuji and N. Katada, *React. Chem. Eng.*, 2020, **5**, 1272–1280.
98 E. P. Barrett, L. G. Joyner and P. P. Halenda, *J. Am. Chem. Soc.*, 1951, **73**, 373–380.
99 (*a*) S. Brunauer, P. H. Emmett and E. Teller, *J. Am. Chem. Soc.*, 1938, **60**, 309–319; (*b*) R. Geyer, J. R. Jambeck and K. L. Law, *Sci. Adv.*, 2017, (3), e1700782.